Subnanogram Mass Measurements on Plasmonic Nanoparticles for Temperature-Programmed Thermal Analysis

ARTICLE *in* JOURNAL OF PHYSICAL CHEMISTRY LETTERS · JANUARY 2010

Impact Factor: 7.46 · DOI: 10.1021/jz900014q

5 AUTHORS, INCLUDING:

Chaoming Wang
Southwest Jiaotong University
36 PUBLICATIONS **233** CITATIONS

SEE PROFILE

Haining Wang
Beihang University(BUAA)
37 PUBLICATIONS **509** CITATIONS

SEE PROFILE

THE JOURNAL OF PHYSICAL CHEMISTRY Letters

pubs.acs.org/JPCL

Subnanogram Mass Measurements on Plasmonic Nanoparticles for Temperature-Programmed Thermal Analysis

Chaoming Wang,[†,‡] Minghui Zhang,[†,#] Haining Wang,[§] Shengli Zou,[§] and Ming Su*[,†,‡]

[†]NanoScience Technology Center, [‡]Department of Mechanical, Materials, and Aerospace Engineering, and [§]Department of Chemistry, University of Central Florida, Orlando, Florida 32826, and [#]Department of Materials Chemistry, College of Chemistry, Nankai University, Tianjin 300071, China

ABSTRACT Ultrasensitive thermogravimetric analysis of adsorbed organic molecules has been achieved on an ordered array of gold nanoparticles used as a novel plasmonic nanobalance. The extinction peaks of the resonating surface plasmon of nanoparticle arrays shift upon loading molecules and return to the original position after a linear temperature rise process. A good correlation exists between the film thickness and magnitude of peak shifts. The detection range of plasmonic nanobalance derived from our results can reach a subnanogram level (1.8 pg on an active area of 100 μm^2), which is much lower than those of mechanical or electronic mass-measuring devices. Such high mass sensitivity, combined with the remote detection capability and high-temperature operation of plasmonic sensors, allows the in situ detections of the masses of loaded material and thermally desorbed molecules.

SECTION Nanoparticles and Nanostructures

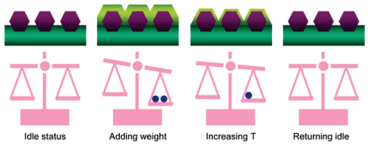

Thermogravimetric analysis (TGA) can determine a material's thermal stability and its fraction of volatile components by monitoring the weight change of the material during programmed temperature rise processes.[1,2] The mass loss recorded by an electronic or mechanical balance is used to derive the point where the mass loss is most apparent.[3] The detection sensitivity of thermogravimetric analysis is strongly dependent on the precision of mass measurements. Historically, precise mass measurements have been achieved in mechanical balances through three designs, a sharp knife edge as frictional-free fulcrum, a long pointer to amplify the deviation of the beam, and a long lever that allows fractional mass to be applied. An electronic balance offers much higher precision and accuracy using a device called a strain gauge load cell.[4] As the cell is compressed, the electrical resistance changes, which is measured by a Wheatstone bridge. In the absence of turbulent airflow, the detection sensitivity of an electronic balance can reach 1 μg at room temperature. As the temperature increases, natural convection from air currents negatively affects the precision. The mass of material can also be measured in dynamic mode, where the resonance frequency of a solid surface or beam shifts once a mass is added on top of it. A quartz crystal microbalance (QCM) can measure the weight of deposited mass at high sensitivity (0.2 μg) under ambient conditions.[5] A microfabricated cantilever operating in dynamic mode can detect as little as 8 ng by reducing the size of vibrating elements.[6] One-dimensional nanomaterials such as nanotubes and nanowires have been proposed as the beams for the dynamic mass measurements.[7−9] Owing to the small mass of a single nanotube or nanowire, the frequency shift upon loading of material will be significant, meaning that the detection sensitivity could be very high to reach single-molecule level. However, the mass readout from a single nanotube/wire is challenging and requires sophisticated techniques such as electron microscopy[10−15] and thus cannot be widely deployed as a practical means for mass measurements. In the case of the microcantilever, loading testing samples on the active area requires a micromanipulator and is often time-consuming.[16] Mostly importantly, the available highly sensitive mass measurement techniques are not compatible with thermal analysis, where the sensing elements cannot survive high temperatures or the temperature effect is nonlinear or too large to identify signals.

The unique optical, magnetic, and chemical properties of nanoparticles have been studied extensively in the past decade. By reducing their diameters to nanometers, nanoparticles with extremely large surface to volume ratios could be potentially used in many areas, including biosensing, catalysis, and functional additives.[17−19] If a certain amount of material can be loaded on an individual nanoparticle or an array of nanoparticles, the property of the nanoparticles will be altered dramatically due to the strong material−nanoparticle

Received Date: September 21, 2009
Accepted Date: October 20, 2009
Published on Web Date: November 06, 2009

DOI: 10.1021/jz900014q | *J. Phys. Chem. Lett.* **2010**, *1*, 79–84

interactions or large material to nanoparticle ratio. Consequently, such a property change of nanoparticles can be read out through an appropriate signal transduction mechanism. Among the most-studied characters, the optical properties of nanoparticles can be used to monitor the interaction between nanoparticles and their surroundings.[20] Instead of utilizing mechanical or electrical approaches to achieve high mass sensitivity, we have used the plasmonic properties of an array of gold nanoparticles to derive the masses of thin films of adsorbed organic molecules, which can be removed by rising the temperature of nanoparticles (Figure 1). In the so-named plasmonic nanobalance, the extinction peaks of the surface plasmon of gold nanoparticles shift linearly as the mass of loaded material increases before reaching the upper limit of mass detection. Upon desorption of materials in a programmed temperature rise process, the extinction peaks of the surface plasmon resonance (SPR) return to the original position. Within the maximal detectable limit, the peak shift is proportional to the mass loaded on the gold nanoparticles. The superior mass sensitivity of the plasmonic nanobalance, combined with the in situ and remote detection capability and high-temperature operation of plasmonic nanosensors, allows the ultrasensitive mass detections and temperature-programmed analysis of loaded organic materials.

As-deposited and thermally annealed gold nanoparticle arrays are imaged at ambient conditions using a multimode atomic force microscope (NanoScope AFM, Veeco) operated in tapping mode. The as-deposited gold nanoparticles are arranged to form hexagonal patterns (Figure 2A), where the average diameter and interparticle distance are about 100 and 230 nm, respectively. The heights of nanoparticles measured from the cross sections of the AFM image are 40 nm. Although some nanoparticles combine with each other and form a long chain, such a structure has optical response in the far-infrared region and will not affect the measurement in the visible wavelength region. After annealing the sample at 600 °C for 10 h, triangle-shaped nanoparticles change to hemispherical shape (Figure 2B). Since the annealing temperature is close to the softening temperature of the Pyrex glass (~750 °C), the annealing process produces semiembedded nanoparticles (Figure 2B inset), where gold nanoparticles are removed by etching in an aqua regia solution for 20 min. The extinction spectra of gold nanoparticles before and after annealing are shown in Figure 2C, where the peak at 563 nm after annealing becomes stronger. X-ray diffraction (XRD) analysis is carried out on a Riguku powder diffractometer using Cu Kα radiation at 40 kV and 30 mA. XRD results of gold nanoparticles annealed at different temperatures show that the diffraction peak of the gold (111) plane becomes stronger after annealing at higher temperatures (Supporting Information Figure S1). The morphologies of partially embedded and crystallized gold nanoparticles are stabilized by a glass matrix. A significant advantage of the plasmonic nanobalance over existing mass measurement techniques is that such a device can be operated directly at high temperature. We have calibrated the temperature effects on the peak shifts. Increasing the temperature at the rate of 5 °C/min leads to

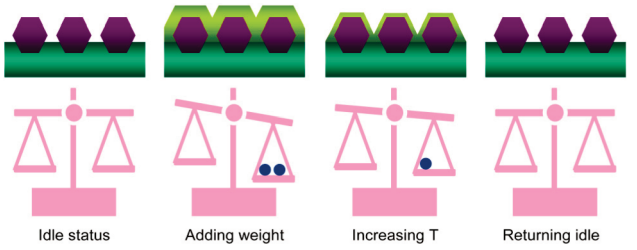

Figure 1. Schematic illustration of an ultrasensitive plasmonic nanobalance.

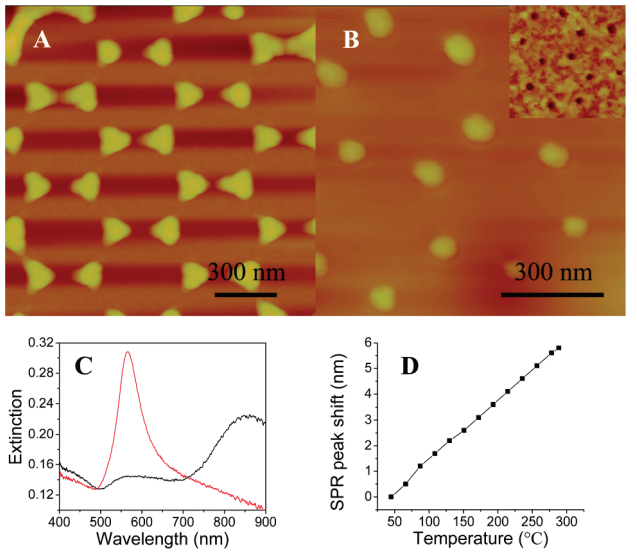

Figure 2. AFM images of gold nanoparticle arrays before (A) and after (B) annealing at 600 °C for 10 h and after removing gold nanoparticles (Figure 2B inset). (C) Extinction spectra of gold nanoparticle arrays before (black curve) and after (red curve) annealing. (D) SPR peak shift versus the temperature.

shifts of the SPR peak of annealed gold nanoparticles to long wavelengths (Figure 2D). The temperature-dependent shift can be understood from the dispersion relation for surface plasmon waves, together with the decrease in the plasmon frequency and increase in the collision frequency in the Drude model as the temperature increases.[21] The SPR peak returns to its original position after the sample is cooled down to room temperature. The processes of the heating−cooling cycle can be repeated many times. The magnitude of peak shifts is linearly proportional to temperature between 20 and 300 °C.[22] Such linear response is the result of structural stability of annealed gold nanoparticles.

In order to derive the mass dependence of the plasmonic nanobalance, thin films of paraffin (melting temperature of 56 °C) are thermally deposited layer-by-layer onto an annealed gold nanoparticle arrays. The thicknesses are controlled by exposing nanoparticles to paraffin vapor for different periods of time (1 to 10 min) and are verified by the height measurement of AFM. A few papers have pointed out the response of SPR to adsorbed layers by calculation and experiments.[23,24] When the thickness of adsorbed layers is much thinner than the characteristic decay length of the electro-

DOI: 10.1021/jz900014q | J. Phys. Chem. Lett. 2010, 1, 79–84

magnetic field, the shift of the SPR extinction peak is proportional to the thickness of adsorbed layers, namely, the linear response regime. For the thicker layers, the peak response to the thickness is beyond the linear regime. In the current experiments, all of the analysis data are based on the linear response regime. As shown in Figure 3A, with the increase of paraffin layer thickness, the SPR peak shifts toward the long wavelength direction, and $\Delta\lambda_{max}$ increases approximately linearly. After depositing a certain number of layers, the $\Delta\lambda_{max}$ stops responding to the layer thickness. Considering the density (0.9 g/cm^3) and molecular weight (228 au) of the paraffin, the maximal measurable mass is about 36 ng, and the detection sensitivity in air can be derived as 0.77 nm/ng in the linear region (Figure 3B). Although the packing density of molecules depends on how fast the film is deposited or whether the film is thermally annealed, the films in our experiment are deposited at relatively slow rate (~4 nm/min); thus, the density of the film could be close to that of bulk material.

The temperature-programmed thermal analysis is carried out by heating gold nanoparticles with paraffin thin films and monitoring SPR signals continuously. Figure 3C shows that the SPR peak shifts toward the short wavelength direction as the temperature increases due to desorption of paraffin molecules. The temperature at which the SPR peak shifts most corresponds to desorption of paraffin. Mass loss kinetics shows a similar trend as that of thermogravimetric analysis; the curves shift to higher temperature at higher heating rate. On the basis of the Arrhenius equation, the thermal mass loss kinetics can be expressed in the following form

$$\frac{d\alpha}{dt} = Af(\alpha)\exp\left(-\frac{E}{RT}\right) \quad (1)$$

where α is the degree of conversion, t is the time, A is the pre-exponential factor, E is the activation energy, R is the gas constant, and $f(\alpha)$ is the differential conversion function. For the nonisothermal conditions with a linear heating program (heating rate is β), the Flynn−Wall−Ozawa isoconversional integral method (FWO) uses the Doyle approximation to approximate the above relation, which gives[25,26]

$$\ln\beta = \ln\frac{AE}{Rg(\alpha)} - 5.331 - 1.052\frac{E}{RT} \quad (2)$$

Thus, at the same mass loss, a plot of ln β versus $-1/T$ should be a straight line, and the activation energy can be derived from the slope. The ln β versus $-1/T$ plots from 20 to 80% conversion for the mass loss of paraffin over gold nanoparticle arrays are shown in Figure 3D, where the effect of temperature on gold nanoparticles has been considered. The lines at different mass loss values are approximately parallel to each other, and all correlation coefficients of linearity are over 0.98. Moreover, the average activation energy calculated from these plots is 32 kJ/mol.

The sensitivity of mass detection is dependent on the nature of materials deposited on the array of nanoparticles. We have studied the shifts of the SPR peak of an array of annealed gold nanoparticles as functions of the thickness of octadecylamine. In contrast to paraffin that has weak interaction with gold, octadecylamine has relatively stronger interaction with gold. As the film becomes thick, the SPR peak shifts linearly in the long wavelength direction until the thickness is 20 nm, where the peak does not shift (Figure 4A). The inset of Figure 4A shows the extinction spectra of gold nanoparticles after exposing to the octadecylamine vapor for different period from 10 to 120 s. The mass detection range (28 ng) is lower than that of the paraffin film, meaning the detection sensitivity is higher. The SPR peak shifts to short wavelength and returns to the original position as the temperature increases linearly (Figure 4B and Supporting Information Figure S2A), suggesting that octadecylamine molecules are desorbed. The desorption is reflected in the intensity change of the SPR peak (Supporting Information Figure S2B), where octadecylamine desorption leads to increase of the transmission magnitude. In the case of thiol molecules that form strong bonds with gold atoms, the sensitivity of mass detection is lower. The surfaces of gold nanoparticles have been modified by 1,10-decanedithiol, and the sample was then heated to high temperature to remove the thiol molecules. Figure 4C shows the shifts of the SPR peak as a function of temperature, where the maximal rate of desorption occurs at 150 °C. Assuming that nanoparticles are hemispheres, the surface area of single gold nanoparticles (radius of 25 nm) available for the self-assembled monolayer (SAM) is calculated to be 3.9×10^{-11} cm^2. Given that the packing density of 1,10-decanedithiol molecules on the gold surface is 4.4×10^{14} cm^{-2},[27] the sensitivity of mass detection is about 125 nm/ng. The detection range depends on the decay length of the electromagnetic field around the nanoparticles. Due to the near-field nature of the surface plasmon, the maximal thickness of a film that can be detected by a plasmonic nanobalance is approximately 20 nm. The maximal detectable mass of a thin film can thus be derived from the density of molecules in thin film. The high mass sensitivity and thermal

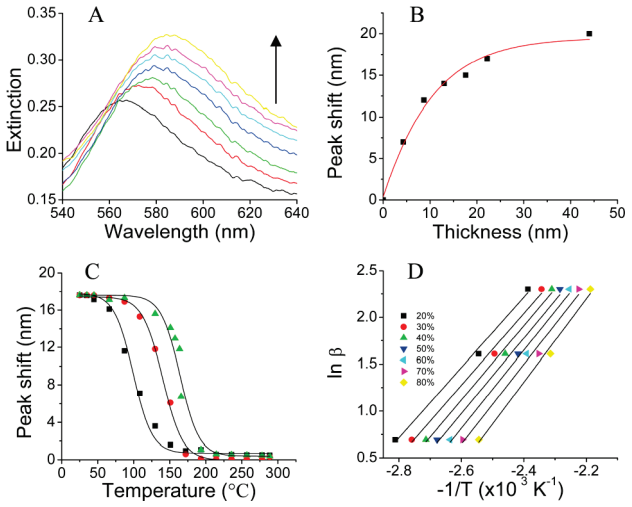

Figure 3. (A) Extinction spectra of gold nanoparticle arrays after exposing to wax vapor for different times. (B) SPR peak shift versus thickness of wax films. (C) SPR peak shift of wax-coated nanoparticles versus the temperature at different heating rates, where the square, circle, and triangle are for results collected at 2, 5, and 10 °C/min. (D) Plot of ln β versus $-1/T$.

DOI: 10.1021/jz900014q | J. Phys. Chem. Lett. 2010, 1, 79–84

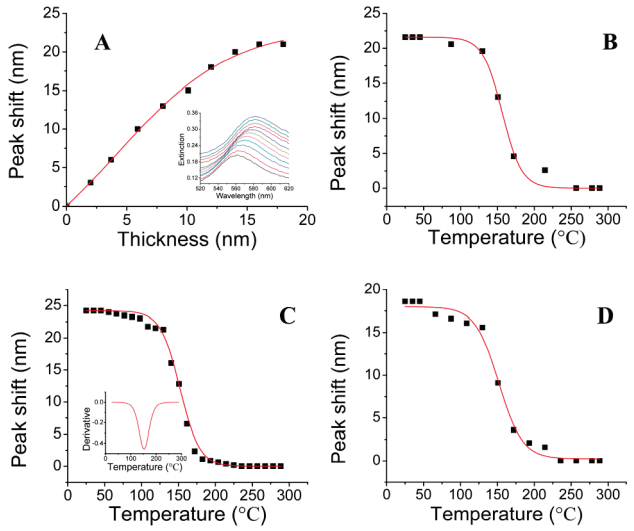

Figure 4. (A) SPR peak shift versus the thickness of octadecylamine thin films; the inset shows extinction spectra of gold nanoparticle arrays after exposure to octadecylamine vapor for different times. SPR peak shifts upon the desorption of octadecylamine (B), 1,10-decanedithiol (C), and 2,4-dinitrotoluene (D) from gold nanoparticles at a heating rate of 5 °C /min. The inset of (C) is the corresponding derivative curve.

analysis ability of the plasmonic nanobalance provides an opportunity to measure the mass of explosive materials. We have used the plasmonic nanobalance to measure the mass of a thin film of 2,4-dinitrotoluene (DNT), which is a derivative of highly explosive 2,4,6-trinitrotoluene (TNT). The thin film of DNT (melting temperature of 71 °C) is thermally deposited on annealed gold nanoparticles. As the deposit time increases, the SPR peak shifts to the long wavelength direction (Supporting Information Figure S2C). Figure 4D shows the peak shifts as a function of temperature, where the maximal desorption occurs at 160 °C. The desorption is also reflected in the change of the SPR peak (Supporting Information Figure S2D), where DNT desorption results in an increase of transmission magnitude. The sensitivity of mass detection is 0.77 nm/ng, which is close to those of paraffin wax and octadecylamine.

At last, the nanobalance can be made of other metals (i.e., silver) and operated in liquid. In this case, polyelectrolyte multilayers are layer-by-layer deposited onto an array of silver nanoparticles. We have used poly(acrylic acid) (PAA) with a molecular weight of 90 000 au and poly(allylamine hydrochloride) (PAH) with a molecular weight of 70 000 au. The multilayers are deposited from 0.01 M solutions of PAA and PAH at pHs of 3.5 and 8.5, respectively. The deposition involves the immersion of charged surfaces (i.e., glass) into the aqueous solutions of polyanions and polycations in an alternating sequence to build multilayers by electrostatic interaction. After each deposition, the SPR peaks of silver nanoparticles are measured in water. Figure 5A shows the extinction spectra of silver nanoparticle arrays in water after depositing 1−10 multilayers, where the peak shifts toward the long wavelength direction after each deposition. After forming seven multilayers, the peak does not shift any more,

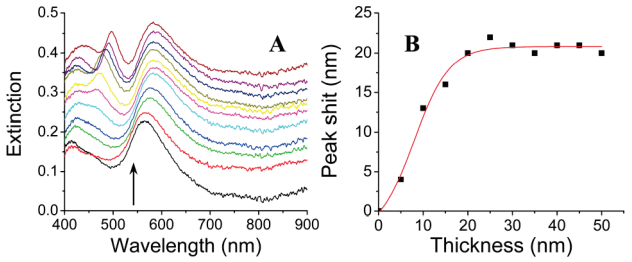

Figure 5. (A) Extinction spectra of silver nanoparticles upon deposition of 1−10 bilayers of PAH/PAA collected in water. (B) The measured (square dots) and simulated (line) peak shifts as functions of the thickness of bilayers.

suggesting saturation of the plasmonic signal. Figure 5B shows the plotted peak shifts versus the thickness of bilayers in water. Before reaching the saturation, the peak shifts show a linear dependence on the thickness of bilayers. Taking the average thickness of one PHA/PAA bilayer of 5 nm, the mass detection sensitivity in the linear region is 0.52 nm/ng in water. The unique ability of mass measurement in liquid could be beneficial for many biological applications such as mass determination of protein molecules.

In our experiment, the surface area is about 2 mm^2, which corresponds to a minimal detection limit of 2 ng of paraffin. Ideally, the active surface area can be reduced down to hundreds of micrometers by making nanoparticle arrays on the end of a multimode optical fiber.[28] Such size reduction will not affect the SPR signal but will lower the detection limit down to the subnanogram level. If a 100 μm diameter optical fiber is used, the mass of paraffin can be as small as 1.8 pg. In the case of thiol, the detection limit could be much smaller. The extremely high mass sensitivity, combined with the remote detection ability and high-temperature operation of the optical sensor, would be a great benefit for temperature-programmed thermal analysis and daily mass measurements. However, due to the surface-sensitive nature of this method, the maximal detectable mass is limited and cannot be used on bulk materials. The maximal operating temperature that can be achieved by this technique is determined by the melting temperatures of gold or silver nanoparticles, which are usually lower than their bulk meting points.[29] In addition, although it can work in the thermogravimetric mode, this technique cannot operate in other thermal analysis modes such as differential thermal analysis or differential scanning calorimetry because the absolute heat flux cannot be measured.

In summary, subnanogram sensitivity has been achieved by a nanoparticle-array-based plasmonic nanobalance for the mass measurements in air and in liquid and temperature-programmed thermal analysis. The plasmonic resonance peaks of nanoparticle arrays shift upon loading materials and return to the original position after a linear temperature rise process. Such high mass detection sensitivity, combined with the remote detection capability and high-temperature operation of the plasmonic sensors, allows the in situ detections of the masses of materials and thermally desorbed molecules and stand-off mass detection of explosive materials.

DOI: 10.1021/jz900014q | J. Phys. Chem. Lett. 2010, 1, 79–84

An ordered array of gold nanoparticles is prepared by nanosphere lithography.[30] In a typical experiment, 2.5 μL of carboxyl-modified polystyrene microsphere (400 nm diameter) solution at 4 wt % concentration (Invitrogen, Carlsbad, CA) is dropped on a clean glass slide that has a thin water film. The existence of the water film can facilitate the packing of microspheres by preventing the fast drying of the suspension. After making the microsphere monolayer, an ordered array of gold nanoparticles is produced by depositing 2 nm of chromium and then 38 nm of gold into the interstitial spaces of densely packed microspheres. The microspheres are removed by sonicating the sample in ethanol for 3 min followed by annealing in an oven at 600 °C for 10 h in air. The SPR measurements are carried out by placing glass slides with nanoparticles in a self-built detection cell that has an inlet and an outlet to allow inert purging gas (nitrogen) to pass. The UV−vis extinction properties of gold nanoparticles are measured by a fiber optical mini spectrophotometer (Ocean Optics, FL) that has a linear array of charge coupled device (CCD) detectors. The multimode optical fiber permits the passage of light in the wavelength range of 400−900 nm. All extinction spectra are collected in transmission mode using normally incident, nonpolarized white light with a Gaussian beam size of 2 mm^2. (Note that the plasmonic active area can be reduced to 100 μm^2 by making nanoparticles on the tip of multimode optical fibers). Each spectrum is an average of 25 individual ones at 10 ms integrations, and the collection is carried out in nitrogen flow. A self-built resistive heating element coupled with a proportional integration−differentiation (PID) controller (JUMO, Germany) is used to heat or cool the detection cell with a predesigned program.

ACKNOWLEDGMENT This work is supported by the King Biomedical Program of the Florida Department of Health and the University of Central Florida. C.W. and M.Z. have equal contribution to this work.

SUPPORTING INFORMATION AVAILABLE XRD spectra of gold nanoparticles deposited on a glass substrate before and after thermal annealing at 300, 400, 500, and 600 °C for 10 h are shown in Figure S1. Extinction spectra of gold nanoparticles coated by octadecylamine and 2,4-dinitrotoluene (DNT) and the effect of the temperature on the transmission change of the coated sample are shown in Figure S2. This material is available free of charge via the Internet at http://pubs.acs.org.

AUTHOR INFORMATION

Corresponding Author:

*To whom correspondence should be addressed. E-mail: mingsu@mail.ucf.edu.

REFERENCES

(1) Jeguirim, M.; Trouvé, G. Pyrolysis Characteristics and Kinetics of Arundo Donax Using Thermogravimetric Analysis. *Bioresour. Technol.* **2009,** *100*, 4026–4031.

(2) Viswanathan, R.; Narasimhan, T. S. L.; Nalini, S. Vapor Pressure Measurements by Mass Loss Transpiration Method with a Thermogravimetric Apparatus. *J. Phys. Chem. B* **2009,** *113*, 8362–8368.

(3) Rhee, Y. M.; Head-Gordon, M. A Delicate Electronic Balance between Metal and Ligand in [Cu−P−Cu−P] Diamondoids: Oxidation State Dependent Plasticity and the Formation of a Singlet Diradicaloid. *J. Am. Chem. Soc.* **2008,** *130*, 3878–3887.

(4) Hanafee, J. E.; Radcliff, S. V. Effect of High Pressure on a Strain Gauge Load Cell. *Rev. Sci. Instrum.* **1967,** *38*, 328–331.

(5) York, R. L.; Holinga, G. J.; Somorjai, G. A. Investigation of the Influence of Chain Length on the Interfacial Ordering of L-Lysine and L-Proline and Their Homopeptides at Hydrophobic and Hydrophilic Interfaces Studied by Sum Frequency Generation and Quartz Crystal Microbalance. *Langmuir* **2009,** *25*, 9369–9374.

(6) Berger, R.; Gerber, C.; Gimzewski, J. K.; Meyer, E.; Guntherodt, H. J. Thermal Analysis Using a Micromechanical Calorimeter. *Appl. Phys. Lett.* **1996,** *69*, 40–42.

(7) Stampfer, C.; Guttinger, J.; Roman, C.; Jungen, A.; Helbling, T.; Hierold, C. Electron Shuttle Instability for Nano Electromechanical Mass Sensing. *Nano Lett.* **2007,** *7*, 2747–2752.

(8) Zhou, J.; Lao, C. S.; Gao, P. X.; Mai, W. J.; Hughes, W. L.; Deng, S. Z.; Xu, N. S.; Wang, Z. L. Nanowire As Pico-gram Balance at Workplace Atmosphere. *Solid State Commun.* **2006,** *139*, 222–226.

(9) Huang, Y. H.; Bai, X. D.; Zhang, Y. In Situ Mechanical Properties of Individual ZnO Nanowires and the Mass Measurement of Nanoparticles. *J. Phys.: Condens. Matter* **2006,** *18*, L179–L184.

(10) Zhao, X. Y.; Hrbek, J.; Rodriguez, J. A. The Decomposition and Chemistry of $Ru_3(CO)_{12}$ on TiO_2(110) Studied with X-ray Photoelectron Spectroscopy and Temperature Programmed Desorption. *Surf. Sci.* **2005,** *575*, 115–124.

(11) Ostblom, M.; Liedberg, B.; Demers, L. M.; Mirkin, C. A. On the Structure and Desorption Dynamics of DNA Bases Adsorbed on Gold: A Temperature-Programmed Study. *J. Phys. Chem. B* **2005,** *109*, 15150–15160.

(12) Millot, B.; Methivier, A.; Jobic, H. Adsorption of n-Alkanes on Silicalite Crystals. A Temperature-Programmed Desorption Study. *J. Phys. Chem. B* **1998,** *102*, 3210–3215.

(13) Kariis, H.; Westermark, G.; Persson, I.; Liedberg, B. Infrared Spectroscopic and Temperature-Programmed Desorption Studies of Dimethylphenylphosphine Adsorbed on the Coinage Metals. *Langmuir* **1998,** *14*, 2736–2743.

(14) Bertilsson, L.; Engquist, I.; Liedberg, B. Interaction of Dimethyl Methylphosphonate with Alkanethiolate Monolayers Studied by Temperature-Programmed Desorption and Infrared Spectroscopy. *J. Phys. Chem. B* **1997,** *101*, 6021–6027.

(15) Engquist, I.; Lundstrom, I.; Liedberg, B. Temperature-Programmed Desorption and Infrared Studies of D_2O Ice on Self-Assembled Alkanethiolate Monolayers: Influence of Substrate Wettability. *J. Phys. Chem.* **1995,** *99*, 12257–12267.

(16) Biswal, S. L.; Raorane, D.; Chaiken, A.; Birecki, H.; Majumdar, A. Nanomechanical Detection of DNA Melting on Microcantilever Surfaces. *Anal. Chem.* **2006,** *78*, 7104–7109.

(17) Fukuba, S.; Tsuboi, K.; Abe, S.; Kajikawa, K. Nonlinear Optical Detection of Proteins Based on Localized Surface Plasmons in Surface Immobilized Gold Nanospheres. *Langmuir* **2008,** *24*, 8367–8372.

(18) Chuang, H.-Y.; Chen, D.-H. Fabrication and Photocatalytic Activities in Visible and UV Light Regions of Ag@TiO_2 and NiAg@TiO_2 Nanoparticles. *Nanotechnology* **2009,** *20*, 105704.

(19) Murugadoss, A.; Chattopadhyay, A. Surface Area Controlled Differential Catalytic Activities of One-Dimensional Chain-Like Arrays of Gold Nanoparticles. *J. Phys. Chem. C* **2008,** *112*, 11265–11271.
(20) Duval Malinsky, M.; Kelly, K. L.; Schatz, G. C.; Van Duyne, R. P. Chain Length Dependence and Sensing Capabilities of the Localized Surface Plasmon Resonance of Silver Nanoparticles Chemically Modified with Alkanethiol Self-Assembled Monolayers. *J. Am. Chem. Soc.* **2001,** *123*, 1471–1482.
(21) Chiang, H. P.; Chen, C. W.; Wu, J. J.; Li, H. L.; Lin, T. Y.; Sánchez, E. J.; Leung, P. T. Effects of Temperature on the Surface Plasmon Resonance at a Metal-Semiconductor Interface. *Thin Solid Films* **2007,** *515*, 6953–6961.
(22) Chiang, H. P.; Yeh, H. T.; Chen, C. M.; Wu, J. C.; Su, S. Y.; Chang, R.; Wu, Y. J.; Tsai, D. P.; Jen, S. U.; Leung, P. T. Surface Plasmon Resonance Monitoring of Temperature via Phase Measurement. *Opt. Commun.* **2004,** *241*, 409–418.
(23) Peterlinz, K. A.; Georgiadis, R. In Situ Kinetics of Self-Assembly by Surface Plasmon Resonance Spectroscopy. *Langmuir* **1996,** *12*, 4731–4740.
(24) Jung, L. S.; Campbell, C. T.; Chinowsky, T. M.; Mar, M. N.; Yee, S. S. Quantitative Interpretation of the Response of Surface Plasmon Resonance Sensors to Adsorbed Films. *Langmuir* **1998,** *14*, 5636–5648.
(25) Flynn, J. H.; Wall, L. A. General Treatment of Thermogravimetry of Polymers. *J. Res. Natl. Bur. Stand., Sect. A* **1966,** *A 70*, 487–523.
(26) Ozawa, T. A New Method of Analyzing Thermogravimetric Data. *Bull. Chem. Soc. Jpn.* **1965,** *38*, 1881–1886.
(27) Li, J.; Liang, K. S.; Camillone Iii, N.; Leung, T. Y. B.; Scoles, G. The Structure of n-Octadecane Thiol Monolayers Self-Assembled on Au(001) Studied by Synchrotron X-ray and Helium Atom Diffraction. *J. Chem. Phys.* **1995,** *102*, 5012–5028.
(28) Villatoro, J.; Monzon-Hernandez, D. Fast Detection of Hydrogen with Nano Fiber Tapers Coated with Ultra Thin Palladium Layers. *Opt. Express* **2005,** *13*, 5087–5092.
(29) Safaei, A.; Shandiz, M. A.; Sanjabi, S.; Barber, Z. H. Modeling the Melting Temperature of Nanoparticles by an Analytical Approach. *J. Phys. Chem. C* **2007,** *112*, 99–105.
(30) Hulteen, J. C.; Treichel, D. A.; Smith, M. T.; Duval, M. L.; Jensen, T. R.; Van Duyne, R. P. Nanosphere Lithography: Size-Tunable Silver Nanoparticle and Surface Cluster Arrays. *J. Phys. Chem. B* **1999,** *103*, 3854–3863.

DOI: 10.1021/jz900014q | *J. Phys. Chem. Lett.* **2010,** *1*, 79–84